


## Spectral Measurement of the Breakdown Limit of $\beta$ -Ga<sub>2</sub>O<sub>3</sub> and Tunnel Ionization of Self-Trapped Excitons and Holes

Md. Mohsinur Rahman Adnan<sup>1,†</sup>, Darpan Verma<sup>2,†</sup>, Zhanbo Xia<sup>1</sup>, Nidhin Kurian Kalarickal<sup>1</sup>,  
Siddharth Rajan<sup>1</sup> and Roberto C. Myers<sup>1,2,\*</sup>

<sup>1</sup>Department of Electrical and Computer Engineering, The Ohio State University, Columbus, Ohio 43210, USA

<sup>2</sup>Department of Material Science and Engineering, The Ohio State University, Columbus, Ohio 43210, USA

 (Received 31 October 2020; revised 21 July 2021; accepted 11 August 2021; published 7 September 2021)

Owing to its strong ionic character coupled with a light electron effective mass,  $\beta$ -Ga<sub>2</sub>O<sub>3</sub> is an unusual semiconductor where large electric fields (approximately 1–6 MV/cm) can be applied while still maintaining a dominant excitonic absorption peak below its ultrawide band gap ( $E_g \sim 4.6$ – $4.99$  eV). This provides a rare opportunity in the solid state to examine exciton and carrier self-trapping dynamics in the strong-field limit at steady state. Under sub-band-gap photon excitation, we observe a field-induced redshift of the spectral photocurrent peak associated with exciton absorption and a thresholdlike increase in peak amplitude at high field associated with self-trapped hole ionization. The field-dependent spectral response is quantitatively fitted with an exciton-modified Franz-Keldysh effect model, which includes the electric-field-dependent exciton-binding energy due to the quadratic Stark effect. Saturation of the spectral redshift with reverse bias is observed exactly at the onset of dielectric breakdown, providing a spectral means to detect and quantify the local electric field and dielectric breakdown behavior in  $\beta$ -Ga<sub>2</sub>O<sub>3</sub>. Additionally, the field-dependent responsivity provides an insight into the photocurrent-production pathway, revealing the photocurrent contributions of self-trapped excitons (STXs) and self-trapped holes (STHs) in  $\beta$ -Ga<sub>2</sub>O<sub>3</sub>. Photocurrent and  $p$ -type transport in  $\beta$ -Ga<sub>2</sub>O<sub>3</sub> are quantitatively explained by field-dependent tunnel ionization of excitons and self-trapped holes. We employ a quantum-mechanical model of the field-dependent tunnel ionization of STXs and STHs in  $\beta$ -Ga<sub>2</sub>O<sub>3</sub> to model the nonlinear field dependence of the photocurrent amplitude. Fitting to the data, we estimate an effective mass of valence-band holes ( $18.8m_0$ ) and an ultrafast self-trapping time of holes (0.045 fs). This indicates that minority-hole transport in  $\beta$ -Ga<sub>2</sub>O<sub>3</sub> can only arise through tunnel ionization of STHs under strong fields.

DOI: [10.1103/PhysRevApplied.16.034011](https://doi.org/10.1103/PhysRevApplied.16.034011)

### I. INTRODUCTION

The conversion of electromagnetic radiation (photon flux) into current density (charge flux) is of fundamental importance in all-solid-state optoelectronics. An electron-hole pair is produced at the location of single-photon absorption, and therefore, the mutual Coulombic bond between photocarriers (exciton) must be broken (dissociation) before carrier separation and collection can take place. However, excitons are generally considered unimportant for understanding the room-temperature optoelectronic response in dominantly covalent ( $sp^3$ -bonded) crystalline semiconductors [1,2]. Traditionally called Wannier-Mott excitons [3,4], the small exciton binding energies ( $E_X < 25$  meV) and small dielectric constants ( $K$ ), combined with light effective masses ( $m^* < 1$ ) of the host material, lead to exciton Bohr radii typically spanning

multiple nearest-neighbor bond lengths ( $a_B > 1$  nm) and are assumed to be fully thermally or electrically dissociated in room-temperature optoelectronics [2,5,6]. The opposite extreme occurs in strongly ionic solids where exciton absorption dominates the optical response with  $E_X > 500$  meV and  $a_B < 0.5$  nm [7,8]. However, ionic crystals with such strongly bonded excitons can hardly be classified as semiconductors, e.g., alkali halides [9,10], with strong electron-lattice coupling strongly limiting charge transport (polarons) [11,12].

More recently, the emergence of two-dimensional (2D) semiconductors with sizable band gaps and light masses, e.g., transition-metal dichalcogenides (TMDs), has demonstrated a regime of exciton physics with simultaneously large  $E_X$  and  $a_B$  [13–16]. Under these conditions, room-temperature optoelectronic properties are dominated by excitons near the band edge. Moreover, charged excitons known as trions become possible, with interesting physics and potential optoelectronic applications [17–21]. Compared with these TMDs, the ultrawide-band-gap ( $\sim 4.6$ – $4.99$  eV [22,23]) semiconductor  $\beta$ -Ga<sub>2</sub>O<sub>3</sub> exhibits

\*myers.1079@osu.edu

<sup>†</sup>Md. M. R. Adnan and D. Verma contributed equally to this work.

similar exciton properties to those of the 2D materials, but with the added tunability associated with its high dielectric breakdown field limit ( $\sim 6\text{--}8$  MV/cm [22–24]) motivating its development for high-power high-field devices and solar-blind ultraviolet photodetectors [23,25–28]. Additionally, these properties enable exploration of steady-state exciton dynamics in the strong-field (nonperturbative) limit, Figs. 1(a) and 1(b).

### A. Exciton Franz-Keldysh (XFK) effect

Band-to-band absorption is altered in the application of an electric field, as characterized by a broadening of the absorption edge below the band gap due to

tunneling-assisted absorption, called the Franz-Keldysh (FK) effect [29,30]. In 1966, Aspnes [31] developed a quantitative model for the field-dependent absorption spectrum within the effective-mass approximation. This model was recently applied by Maeda *et al.* to quantitatively model the absorption phenomenon at constant excitation wavelength with varying applied field in wide-band-gap semiconductors like SiC- and GaN-based devices [32–35]. Sub-band-gap absorption in GaN gives rise to excitons that must be dissociated before any photocurrent can be measured [36], but the Aspnes model ignores exciton absorption and is therefore only valid in GaN for a limited range of wavelengths and fields. Theoretical work by Dow and Redfield [37], Blossey [38], and Merkulov [39] showed

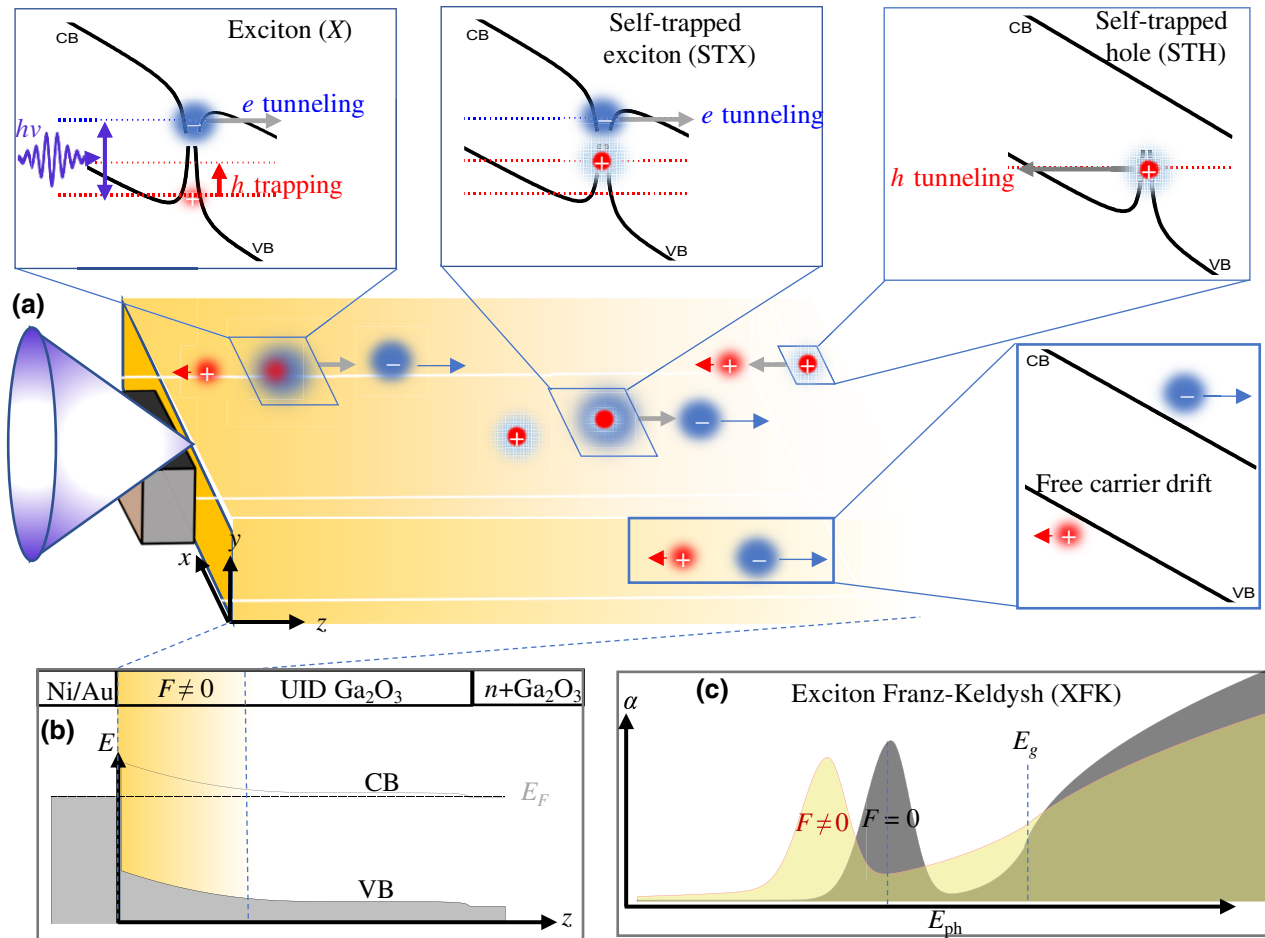


FIG. 1. Electric-field-modified exciton absorption, dissociation, and carrier-ionization processes in the depletion region of a  $\beta$ -Ga<sub>2</sub>O<sub>3</sub> Schottky barrier diode. (a) Photon flux is focused to a point  $(x, y)$  on the device surface, while an applied reverse bias and Schottky barrier cause a depleted region with a nonzero electric field ( $F$ ) along the  $z$  axis. Absorbed sub-band-gap photons generate neutral free excitons ( $X$ ) formed by Coulombic electron and hole interaction, and different ionization processes take place, leading to photocurrent from drifting free carriers.  $F$  distorts the conduction-band (CB) and valence-band (VB) edges, which allows  $e$ -tunneling-based dissociation of  $X$ . Within  $X$ , holes generate a lattice distortion that locally binds holes, generating neutral self-trapped excitons (STXs), which themselves can dissociate by  $e$  tunneling. Afterward, a self-trapped hole (STH) is left behind. For these immobile charges to contribute to current, they must be field ionized by  $h$  tunneling out of the trapping potential. (b) Band-edge diagram of the Schottky diode structure and layer structure. (c) Schematic of absorption coefficient ( $\alpha$ ) modified by  $F$ , the Franz-Keldysh effect. Sub-band-gap  $X$  absorption peak is redshifted with the field, whereas the band-edge absorption edge shows field-induced broadening.

that the electron-hole Coulombic bond (exciton) led to a qualitatively distinct electroabsorption behavior from the FK effect, namely, a sub-band-gap absorption peak that shifted under an applied field, which we refer to as the XFK effect, Fig. 1(c). Exciton absorption is observed in the FK effect in GaN [40,41], revealing an exciton peak structure near the band edge in GaN absorption spectra, which redshifts with increasing applied field. We recently reported the experimental observation and quantitative modeling of the XFK effect in the photocurrent spectral response of GaN [36], which demonstrates a spectral measurement of the local electric field and a route to develop all-optical electric field microscopy to explore breakdown physics and refine electrostatic modeling for high-field devices. However, in the case of GaN,  $E_X \sim 20.3\text{--}27$  meV [36] is modest ( $\sim k_B T$ ), and therefore, the XFK peak is only resolvable at room temperature at relatively low electric fields, since the excitons are easily dissociated [40,41]. By contrast, excitons in TMDs and  $\beta$ -Ga<sub>2</sub>O<sub>3</sub> fully dominate the sub-band-gap absorption, an effect accentuated in the latter by the weak band-to-band absorption of its indirect band gap [42–44].

### B. Similarity of excitons in 2D TMDs and $\beta$ -Ga<sub>2</sub>O<sub>3</sub>

Because excitons are electrically neutral, a photocurrent is obtained only from strongly bound excitons if a sufficiently large electric field is applied to dissociate them into mobile conduction-band electrons and valence-band holes via tunnel ionization [45–49], as illustrated in Fig. 1(a); otherwise, the excitons would decay through electron-hole recombination. The tunneling barrier height and width are modified by an expected increase in the binding energy with field due to the Stark effect [13–15, 40,41,50–52]. Such field-ionization phenomena are well studied in organic semiconductors [52,53], but for inorganic solid-state systems are typically limited to discussions of impurity ionization in the low-field (perturbative) regime [40,41,49]. Only very recently have such high-field exciton-dissociation processes been described in a group of inorganic solid-state systems i.e., in TMD materials [13–15,50,51]. For example, in the layered semiconductor WSe<sub>2</sub> with  $E_X = 170$  meV, the bias-dependent photocurrent amplitude is explained in terms of a Stark-modified exciton-binding energy, see the Supplemental Material of Ref. [14]. *Ab initio* Bethe-Salpeter equation (BSE) calculations can predict the band gap correctly only if dielectric screening effects of several hexagonal boron nitride layers are included but fail to predict the correct  $E_X$ , while a screened Wannier-Mott model can explain the observed  $E_X$ . Previously, numerical and analytical models for quantitative field-induced dissociation rates for different TMDs showed the dependence of exciton dissociation on the anisotropic dielectric screening environment [17,50,54–59], where the in-plane electron-hole potential follows  $1/r$

potential over long range, but a weaker logarithmic divergence over short range due to screening [37,38]. More recently, Kamban and Pedersen treated excitons as 2D hydrogen atoms confined in plane within a given screening distance to model exciton dissociation and Stark effects in TMDs [50].

Similar 2D-like hydrogenic excitons appear to be present in  $\beta$ -Ga<sub>2</sub>O<sub>3</sub>. The optical anisotropy of  $\beta$ -Ga<sub>2</sub>O<sub>3</sub> was demonstrated experimentally by Onuma *et al.* in an electroreflectance study [43], and further *ab initio* calculations [density functional theory in the GW approximation (DFT + GW)] by Furthmüller and Bechstedt [44] showed that O<sup>2-</sup> 2*p* valence-band states (holes) of  $\beta$ -Ga<sub>2</sub>O<sub>3</sub> coupled with Ga<sup>3+</sup> 4*s* conduction-band states (electrons) formed anisotropic (2D-like) excitons; absorption energies for *s* - *p<sub>x</sub>* (*a*-axis polarized) and *s* - *p<sub>z</sub>* (*c*-axis polarized) are about 0.3 eV larger than that along *s* - *p<sub>y</sub>* (*b*-axis polarized). Exciton wave functions in  $\beta$ -Ga<sub>2</sub>O<sub>3</sub>, therefore, exhibit 2D anisotropy: weakly bound with large wave functions along the *b* axis [010] and tightly bound with a small wave function within the *a*-*c* plane (010). This pseudo-2D behavior of excitons in  $\beta$ -Ga<sub>2</sub>O<sub>3</sub> is further corroborated by the BSE calculations of Varley and Schleife [42], showing a strong exciton absorption at lower energy for photons polarized along the *a* (*x*) or *c* (*z*) axis, compared with that along the *b* (*y*) axis. Just like TMDs, a screened Mott-Wannier model for estimating the correct  $E_X = 270$  meV must be used for  $\beta$ -Ga<sub>2</sub>O<sub>3</sub> [60]. Beschedt *et al.* showed that, due to the strong exciton-binding energy (larger than optical phonon energies), lattice screening of the electron-hole interaction was greatly reduced in comparison with what was expected from the static dielectric constant. Similar to TMDs,  $\beta$ -Ga<sub>2</sub>O<sub>3</sub> exhibits a large  $E_X$  ( $\sim 180\text{--}270$  meV [60–62]) and anisotropic (2D-like) optical response, as predicted from the BSE calculations of its absorption spectra by Varley and Schleife [42]. Due to the anisotropic dielectric environment, similarly large exciton polarizabilities (induced dipole) are expected [50], such that the exciton-binding energy is strongly field dependent (Stark effect).

### C. Exciton Stark effect and tunnel ionization of self-trapped holes in $\beta$ -Ga<sub>2</sub>O<sub>3</sub>

Similar to polarons ubiquitous to many ionic materials [63],  $\beta$ -Ga<sub>2</sub>O<sub>3</sub> exhibits carrier self-trapping, where, due to the large effective mass of the holes, they are localized to a few bond lengths, leading to a strong lattice distortion. A valence-band hole centered at an O<sup>2-</sup> site will push Ga<sup>3+</sup> nearest neighbors outward and draw O<sup>2-</sup> next-nearest neighbors inwards, forming a trapping potential ( $\sim 490$  meV [64]) that then localizes the hole even further. These STHs are thought to limit the *p*-type conductivity in  $\beta$ -Ga<sub>2</sub>O<sub>3</sub>. Under optical absorption, the STHs together with free electrons form STXs, which demonstrate a

high binding energy ( $\sim 680$  meV [64]) similar to that of alkali-halide excitons. Yamaoka *et al.* observed STXs and STHs in the optical response of  $\beta$ -Ga<sub>2</sub>O<sub>3</sub> [64–66]. These STXs and STHs must be field ionized if a photocurrent is to be obtained from  $\beta$ -Ga<sub>2</sub>O<sub>3</sub> devices, Fig. 1(a).

Here, we present measurements of  $\beta$ -Ga<sub>2</sub>O<sub>3</sub> exciton-absorption and -dissociation processes in the strong-field regime. A photocurrent spectral peak associated with exciton absorption redshifts under reverse bias due to the XFK effect. The spectral response is explained by including the quadratic field dependence of the exciton-binding energy, the exciton Stark effect. The model predicts a continuous redshift of the exciton peak with field; however, data reveal a saturation effect, where the spectral redshift halt due the onset of breakdown, in agreement with previously reported estimates for the breakdown field ( $\sim 6$  MV/cm [23,24]). Using the spectral peak position as an electric field sensor, we examine the photocurrent-peak-amplitude response as a function of field. A high-field threshold behavior is observed, with turn on at about 4.5 MV/cm. The peak-amplitude changes are interpreted to be due to the field-dependent quantum efficiency (ratio of photocarriers collected to photons absorbed) associated with the exciton and STH ionization processes. We adapt a field-ionization model of quasi-bound state tunneling to describe the exciton-dissociation process in  $\beta$ -Ga<sub>2</sub>O<sub>3</sub>. Using literature values of minority-carrier lifetimes and carrier mobilities, we derive field-dependent rate equations for dissociation, ionization, and photocarrier transport. The nonlinear field dependence of the photocurrent is fitted using two free parameters: the valence-band hole effective mass and the self-trapping time of holes. The determined values agree with theoretical band-structure estimates for the valence-band effective mass [60,61] and recent ultra-fast measurements of self-trapped holes [67].

## II. FIELD-INDUCED REDSHIFT OF EXCITON-ABSORPTION PEAK

Figure 1(b) shows the structure of the  $\beta$ -Ga<sub>2</sub>O<sub>3</sub> Schottky barrier diode (SBD) used for our study. Epitaxial growth of  $\beta$ -Ga<sub>2</sub>O<sub>3</sub> is carried out using plasma-assisted molecular-beam epitaxy (Riber MBE Control Solutions M7). Slightly-Ga-rich growth conditions are used for the growth of  $\beta$ -Ga<sub>2</sub>O<sub>3</sub> at a Ga beam equivalent pressure (BEP) of  $8 \times 10^{-8}$  Torr, an oxygen pressure during growth of  $1.5 \times 10^{-5}$  Torr, a plasma power of 300 W, and  $T_{\text{sub}} = 630^\circ\text{C}$  (pyrometer). The epitaxial structure for the SBD consists of an unintentionally doped (UID) Ga<sub>2</sub>O<sub>3</sub> layer of 1  $\mu\text{m}$  thick grown on a Sn : Ga<sub>2</sub>O<sub>3</sub> (010) substrate [22,68] (Tamura). The Schottky top contacts are formed by evaporating a Ni/Au (30 nm/100 nm) metal stack, while the ohmic bottom contacts are a Ti/Au (50 nm/100 nm) metal stack annealed at 470  $^\circ\text{C}$  for 1 min. As shown in the band

diagram in Fig. 1, the UID Ga<sub>2</sub>O<sub>3</sub> layer has an average doping concentration of  $5 \times 10^{17} \text{ cm}^{-3}$ , as obtained from  $C$ - $V$  measurements. Beyond the UID layer, the doping concentration is slightly higher, i.e.,  $1 \times 10^{18} \text{ cm}^{-3}$ . The energy band diagram calculated from one-dimensional (1D) Poisson solver [69,70] in Fig. 1(b) demonstrates that almost all applied potential drops within the 1- $\mu\text{m}$ -thick UID layer. The experimental setup for photocurrent spectral measurements is the same as that described in Ref. [36]. A chopped Xe lamp coupled to a monochromator serves as the photon-energy ( $E_{\text{ph}}$ ) tunable pulsed photoexcitation that is focused using a reflective microscope objective (40 $\times$ ) onto the SBD, generating a photocurrent, which is acquired with a lock-in amplifier.

The device and experimental geometry are shown in Fig. 2(a), where the crystallographic axes of the monoclinic  $\beta$ -Ga<sub>2</sub>O<sub>3</sub> crystal are shown, as well as the two positions ( $P1$  and  $P2$ ) of local photocurrent spectroscopy. Representative photoresponsivity spectra for  $\beta$ -Ga<sub>2</sub>O<sub>3</sub> (at  $P1$ ) are shown in Figs. 2(b) and 2(c) at various values of reverse bias. The spectral variation in the absorption due to applied reverse bias ( $V_{\text{expt.}}$ ) is qualitatively different for the  $\beta$ -Ga<sub>2</sub>O<sub>3</sub> device than what is observed in other wide-band-gap semiconductors [33,36,40,41]. GaN shows an XFK-induced redshift of the optical absorption edge along with spectral broadening as the bias increases [36]. This increased sub-band-gap absorption broadening is typical of the band-edge FK effect. In contrast,  $\beta$ -Ga<sub>2</sub>O<sub>3</sub> shows an XFK-like redshift of the exciton peak with increasing bias [Fig. 2(b)], but without any apparent spectral broadening [Fig. 2(c)]. Additionally, unlike most semiconductors, the photocurrent does not increase strongly above the band gap (4.99 eV), but instead shows reduced absorption. This spectral behavior is consistent with the literature on excitonic absorption examined both theoretically and experimentally. The characteristic exciton peak of  $\beta$ -Ga<sub>2</sub>O<sub>3</sub> is predicted by solutions of the BSE [42]. *Ab initio* calculations of the imaginary part of the dielectric function of  $\beta$ -Ga<sub>2</sub>O<sub>3</sub> have been carried out in Ref. [42] both with and without accounting for the  $e$ - $h$  interaction. Without the exciton effect, the absorption response is a slow increase due to the indirect band gap. Only when the  $e$ - $h$  interaction is accounted for is a strong excitonic peak observed below the band gap. The excitonic peaks were also observed from spectroscopic ellipsometry measurements in the imaginary part of the dielectric function by Sturm *et al.* [62].

As described in Sec. I B, one of the signature features of exciton absorption in  $\beta$ -Ga<sub>2</sub>O<sub>3</sub> is anisotropic absorption. Therefore, to further confirm the excitonic origin of the photocurrent peak, we utilize a linear polarizer ( $\alpha$ -BBO, BaB<sub>2</sub>O<sub>4</sub>) connected to a motorized rotation stage to measure the polarization dependence of the photocurrent peak position. X-ray diffraction is first used to determine the in-plane crystallographic orientation of the device.



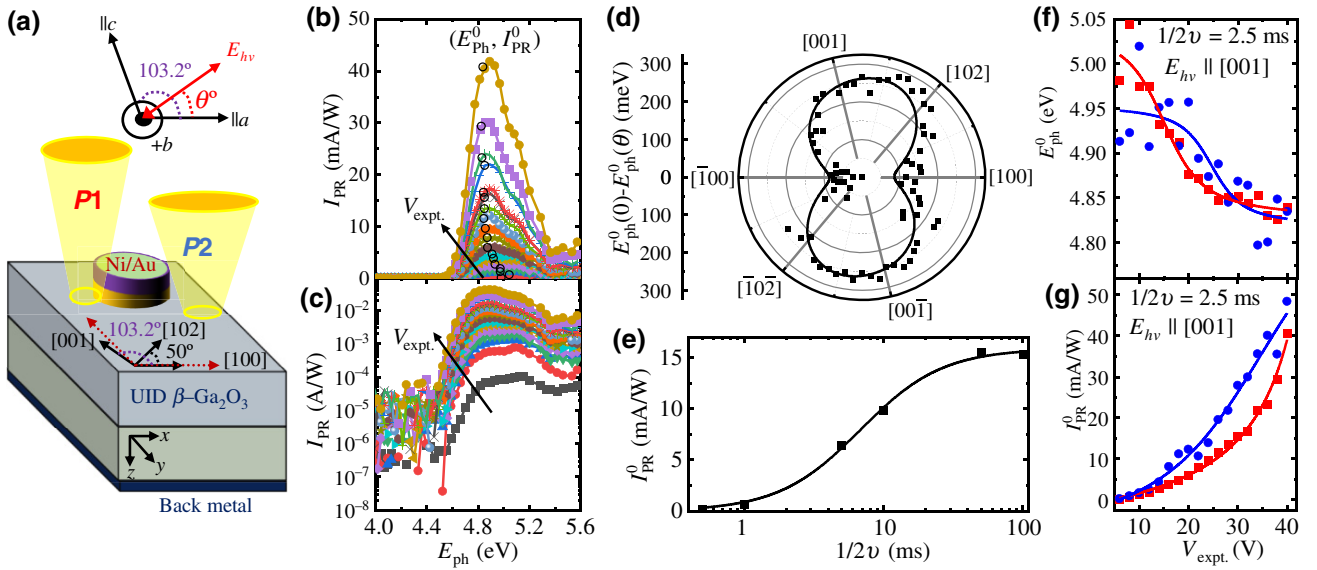


FIG. 2. Polarization- and frequency-dependent photocurrent spectroscopy of  $\beta$ -Ga<sub>2</sub>O<sub>3</sub> Schottky diodes. (a) Schematic of device structure on a  $\beta$ -Ga<sub>2</sub>O<sub>3</sub> (010) oriented crystal, and excitation geometry showing the polarization angle and crystallographic axes. (b) Representative photocurrent spectra normalized by excitation power (photoresponsivity,  $I_{PR}$ ) at various values of reverse bias ( $V_{\text{expt}}$ ). Black circles indicate peaks in  $I_{PR}$  fitted by a “bi-Gaussian” peak-fitting routine. (c) Same data plotted on a semilogarithmic scale. (d) Polarization-angle ( $\theta$ ) dependence of the photocurrent peak position ( $E_{\text{ph}}^0$ ) relative to the peak position at  $\theta = 0^\circ$  (parallel to [100]), revealing the anisotropy of exciton absorption in  $\beta$ -Ga<sub>2</sub>O. Line is a guide to the eye. (e) Peak amplitude ( $I_{PR}^0$ ) as a function of illumination time (plotted on a semilogarithmic scale). (f) Peak position ( $E_{\text{ph}}^0$ ) as a function of  $V_{\text{expt}}$ . (g) Peak amplitude ( $I_{PR}^0$ ) as a function of  $V_{\text{expt}}$ .

Photocurrent spectra are collected at a reverse bias of 30 V with the polarizer angle ( $\theta$ ) stepped every  $5^\circ$  for  $360^\circ$ , where  $\theta = 0$  is aligned along the  $a$ -axis [100] direction. The peak position of the photocurrent spectra ( $E_{\text{ph}}^0$ ) are extracted by fitting the peaks to a bi-Gaussian function. The peak redshift [ $E_{\text{ph}}^0(0) - E_{\text{ph}}^0(\theta)$ ] relative to the  $a$ -axis position is plotted in polar coordinates as a function of polarizer angle ( $\theta$ ) in Fig. 2(d), where the high-symmetry crystal axes are labeled. As expected, for this (010) plane, in  $\beta$ -Ga<sub>2</sub>O<sub>3</sub>, the exciton absorption peak shows twofold rotational symmetry. Within the  $a$ - $c$  plane (010) the  $a$ -axis orientation shows the highest-energy absorption. Data show the maximum redshift along the [001] and [102] axes, reproducing the anisotropic exciton absorption in  $\beta$ -Ga<sub>2</sub>O<sub>3</sub> previously reported through both experiments and theory [42–44],

From Fig. 2(b), we observe that the responsivity peak amplitudes ( $I_{PR}^0$ ) are smaller than those reported in previous works [27,28,71]. In these studies, the amplitudes are larger than what is allowed by the theoretical limit of photocurrent generation due to a proposed gain mechanism, where the Schottky barrier gets lowered by positive charge (self-trapped hole) building up at the metal-semiconductor interface [27,28]. In these studies, UV illumination is modulated at a slow rate,  $< 1$  Hz, and the unusually large responsivities appear to charge up over  $> 100$  ms timescales, corresponding to interface charge

buildup. In our experiments, we modulate the excitation at about 200 Hz to eliminate these slow dynamics. To confirm that this is indeed the case, we carry out photocurrent spectroscopy as a function of illumination time. Figure 2(e) shows the peak amplitude ( $I_{PR}^0$ ) dependence on illumination time,  $1/2\nu$  (ms), where  $\nu$  is the chopper frequency. In Ref. [27], hole trapping and positive charge buildup happen only when the junction is under UV illumination for an extended period of time,  $> 100$  ms [72]. As can be observed from Fig. 2(e), the responsivity increases strongly for timescales approaching 100 ms, whereas the gain mechanism can be ignored for illumination times of  $< 5$  ms.

To examine the field dependence of the photocurrent spectra, bias-dependent measurements are performed while focusing the light source on two different spots of the device: at the edge of the top electrode ( $P1$ ) and at a displacement along the  $c$  axis from the top electrode ( $P2$ ), with excitation polarized along the  $c$  axis [Fig. 2(a)]. Since the reverse bias is applied at the top electrode, the potential drop and field variation are expected to be larger at  $P1$  than at  $P2$ .  $E_{\text{ph}}^0$  and  $I_{PR}^0$  are plotted as a function of  $V_{\text{expt}}$  for data taken at  $P1$  (red) and data taken at  $P2$  (blue) in Figs. 2(f) and 2(g), respectively. At both positions, we observe a redshift of  $E_{\text{ph}}^0$  [Fig. 2(f)] with no qualitative difference in behavior for the two positions within the noise of peak fitting.  $P1$  (red, near electrode) has a larger

range of variation in peak position than  $P2$  (blue, far from electrode), which is indicative of a higher local  $F_{\max}$ .  $I_{\text{PR}}^0$  shows a nonlinear increase with bias [Fig. 2(g)].

### A. Photoresponsivity and field-dependent absorption coefficient

To understand the photoresponsivity behavior, we note that the SBD is a vertical device with probes placed on the top and bottom metal electrodes. If the photon flux incident on the top electrode is  $\varphi_0$ , then the flux entering  $\beta\text{-Ga}_2\text{O}_3$  is  $(1-r)\varphi_0$ , where  $r$  is the reflectance of the top electrode-semiconductor layer. After absorption in the depletion region, the photon flux exiting the depletion region and entering nondepleted  $\beta\text{-Ga}_2\text{O}_3$  is  $(1-r)\varphi_0 e^{-\int_0^W \alpha_{\text{XFK}}[F(z), E_{\text{ph}}] dz}$ , where  $\alpha_{\text{XFK}}[F(z), E_{\text{ph}}]$  is the field- and  $E_{\text{ph}}$ -dependent XFK absorption coefficient,  $F(z)$  is the vertical component of the electric field versus depth ( $z$ ), and  $W$  is the depletion width. Since the nondepleted layer has a negligible electric field, photocarriers can only be produced and collected within the minority hole-diffusion length,  $L_n$ , with an absorption factor of  $e^{-\alpha_n L_n}$ , where  $\alpha_n$  is the absorption coefficient of  $n$ -doped  $\beta\text{-Ga}_2\text{O}_3$ . Because the absorption coefficient of  $\beta\text{-Ga}_2\text{O}_3$  is quite small below the band gap ( $<1000 \text{ cm}^{-1}$ ) [73] and the minority hole-diffusion length,  $L_n$ , is only about 200–300 nm [74], then  $e^{-\alpha_n L_n} \sim 1.000$ , and we can fully neglect photocurrent produced in this region. Absorption in the nondepleted  $n$ -type  $\beta\text{-Ga}_2\text{O}_3$  layer ( $L \sim 500 \mu\text{m}$ ) reduces the photon flux incident on the back surface to about  $e^{-\alpha_n L} > e^{-1000 \times 0.05}$ , which, together with the diffuse hemispherical reflection off the back surface of the substrate, allows us to ignore absorption due to a second optical pass through the depletion region. Within the depletion region of the Schottky diode, where almost all the voltage drops, the absorbed photon flux (converted into excitons) is  $(1-r)\varphi_0 \left\{ 1 - e^{-\int_0^W \alpha_{\text{XFK}}[F(z), E_{\text{ph}}] dz} \right\}$ . Thus, the photocurrent density generated in the SBD will be,

$$I_{\text{PC}} = \eta q (1-r) \varphi_0 \left\{ 1 - e^{-\int_0^W \alpha_{\text{XFK}}[F(z), E_{\text{ph}}] dz} \right\}, \quad (1)$$

where  $\eta$  is the internal quantum efficiency (IQE), representing the ratio of carriers collected to photons absorbed, and  $q$  is the electron charge [72]. Normalizing the photocurrent with respect to the measured wavelength-dependent input-power density ( $E_{\text{ph}}\varphi_0$ ) gives the photoresponsivity,  $I_{\text{PR}}$  (A/W):

$$I_{\text{PR}} = \frac{I_{\text{PC}}}{E_{\text{ph}}\varphi_0} = \frac{\eta q (1-r) \left\{ 1 - e^{-\int_0^W \alpha_{\text{XFK}}[F(z), E_{\text{ph}}] dz} \right\}}{E_{\text{ph}}}. \quad (2)$$

The  $r$  spectrum of the SBD device is measured over the range  $E_{\text{ph}}=3.6 \text{ eV}$  to  $5 \text{ eV}$  and found to be roughly

constant,  $r = 0.15 \pm 0.04$ . In modeling  $I_{\text{PR}}$ , we therefore assume a constant value of the prefactor,  $(1-r)=0.85$  [72]. Therefore, it has no impact on the  $E_{\text{ph}}$  dependence of  $I_{\text{PR}}$ , which depends only on the average absorption coefficient in the depletion layer, the depletion width, and the quantum efficiency.

### B. Stark-modified XFK effect in $\beta\text{-Ga}_2\text{O}_3$

$\beta\text{-Ga}_2\text{O}_3$  has an exciton binding energy of  $E_x^0 = 180 - 270 \text{ meV}$  [60–62] at zero applied field ( $F=0$ ). The binding energy increases with electric field due to the Stark effect,  $E_x = E_x^0 + bF^2$ , where  $b = (9q^2 a_B^2 / 8E_x^0)$  is the polarizability [52]. Here,  $a_B = a_0 K m_0 / \mu_{\text{ex}}$  is the exciton Bohr radius,  $a_0$  (approximately 53 pm) is the Bohr radius of hydrogen, and  $E_x^0 = 13.6 \mu_{\text{ex}} / (m_0 K^2)$ , where  $\mu_{\text{ex}}$  is the exciton reduced mass and  $K$  is the static dielectric constant, which strongly influences the polarizability,  $b$ . Bechstedt and Furthmüller developed a modified Wannier-Mott exciton model for  $\beta\text{-Ga}_2\text{O}_3$ , which incorporates an effective dielectric constant ( $K^* \sim 3.99$ ) that considers the LO-phonon charge-carrier screening at optical frequencies and the anisotropic effective mass [60]. This modified Wannier-Mott exciton model captures the experimentally determined values of  $E_x$  of  $\beta\text{-Ga}_2\text{O}_3$ .  $K$  ( $K^*$ ) is the static (effective) dielectric constant, which equals 14.82 (3.99) [60];  $\mu_{\text{ex}} = 0.3 m_0$  [60]. Using  $a_B \sim 0.70 \text{ nm}$  and  $E_x^0 \sim 250 \text{ meV}$ , we calculate  $b = 2.1 \times 10^{-18} \text{ eV}(\text{m/V})^2$ , which is of the same order of magnitude as that for several TMDs, see Table II of Ref. [50]. Notably, the predicted Stark shift of  $\beta\text{-Ga}_2\text{O}_3$  traverses a similar range to that found in TMD materials for the range of applied fields ( $\leq 0.5 \text{ MV/cm}$ ) of Ref. [50].

The field-dependent exciton-absorption coefficient,  $\alpha_{\text{XFK}}[F(z), E_{\text{ph}}]$ , is given by Merkulov [39]

$$\alpha_{\text{XFK}}[F(z), E_{\text{ph}}] = Cx/\pi^2 (\delta^2 x^2 + 1), \quad (3)$$

with  $x = (8/f) e^{[-(4/3)(\Delta^{3/2}/f) - (2/\sqrt{\Delta}) \ln(8\Delta^{3/2}/f)]}$ ,  $\delta = \Delta - 1 - (9f^2/2)$ ,  $f = qF(z)a_B/E_x$ ,  $\Delta = (E_g - E_{\text{ph}})/E_x$ , where  $C$  is a normalization constant that is the same as that for the free carrier case [75], such that it does not affect the peak shift. Employing this quantitative model, we utilize  $E_g = 4.99 \text{ eV}$  [76],  $E_x^0 = 270 \text{ meV}$  [61], and  $\mu_{\text{ex}} = 0.3 m_0$  [60], with  $a_B \cong 0.70 \text{ nm}$  and  $K^* = 3.99$  [60].

### C. Spectral observation of the breakdown limit of $\beta\text{-Ga}_2\text{O}_3$

The electric field profile is well approximated by a triangle, typical for Schottky diodes:

$$F(z) = F_{\max} \left( \frac{W-z}{W} \right), \quad (4)$$

where  $W$  (in  $\mu\text{m}$ ) is the depletion width given by  $W = [2(V_{\text{expt.}} + V_{\text{BI}})]/F_{\max}$ ,  $V_{\text{expt.}}$  is the applied reverse bias,

$V_{\text{BI}} = \varphi_B - (k_B T/q) \ln(N_c/N_d)$  is the built-in potential barrier of the  $Ni/Au/\beta$ -Ga<sub>2</sub>O<sub>3</sub> SBD,  $\varphi_B = 1.23$  V [77] is the barrier height,  $N_c = 3.72 \times 10^{18} \text{ cm}^{-3}$  [78] is the effective density of states for the conduction band,  $N_d = 5 \times 10^{17} \text{ cm}^{-3}$  is the UID-layer donor concentration, and  $F_{\text{max}}$  is the field maximum at the Schottky junction. Due to electrostatic variation, it is possible that the field profile changes from the idealized picture, leading to varying  $F_{\text{max}}$  and/or  $V_{\text{expt.}}$ ; thus, we explore the spectral sensitivity of  $I_{\text{PR}}$  to such variations in the field profile. First, holding  $V_{\text{expt.}}$  constant,  $F_{\text{max}}$  is varied to change the field description  $F(z)$ , as shown in Fig. 3(a). Second, keeping  $F_{\text{max}}$  constant,  $V_{\text{expt.}}$  is varied, Fig. 3(b). For all field profiles, the depletion width is determined by the electrostatic requirement that  $V_{\text{expt.}} = \int_0^W F(z) dz$ .

Using Eqs. (2)–(4), the  $I_{\text{PR}}$  spectra are calculated assuming  $\eta = 1$  and plotted in Figs. 3(c) and 3(d) for the two different electrostatic conditions shown in Figs. 3(a) and 3(b), respectively. First, we note that the Stark-modified XFK model of  $I_{\text{PR}}$  shows the peak-shaped spectrum for sub-band-gap energies, in agreement with experimental data for  $\beta$ -Ga<sub>2</sub>O<sub>3</sub> [Fig. 2(a)]. In the case of varying  $F_{\text{max}}$  and constant  $V_{\text{expt.}}$  [Fig. 3(a)], the modeled  $I_{\text{PR}}$  spectra in Fig. 3(c) show a redshift of the  $I_{\text{PR}}$  peak with  $F_{\text{max}}$ . For the  $F(z)$  profile of Fig. 3(b), where  $F_{\text{max}}$  is constant (2 MV/cm) but  $V_{\text{expt.}}$  is adjusted from 10 to 40 V, the  $I_{\text{PR}}$  spectra show no clear variation [Fig. 3(d)]. Thus, the peak positions of

the  $I_{\text{PR}}$  spectra ( $E_{\text{ph}}^0$ ) depend solely on  $F_{\text{max}}$  and exhibit no dependence on  $V_{\text{expt.}}$ . This demonstrates that, for  $\beta$ -Ga<sub>2</sub>O<sub>3</sub> SBDs, the photocurrent spectra are apparently insensitive to absorption in the low-field regions.

From the modeled spectra, we numerically determine the relationship between  $F_{\text{max}}$  and  $E_{\text{ph}}^0$  to calibrate  $E_{\text{ph}}^0$  as a spectral field sensor. Peak position is determined by bi-Gaussian peak fits to the modeled  $I_{\text{PR}}$  spectra shown in Fig. 3(c), and the determined  $E_{\text{ph}}^0$  values are plotted as a function of  $F_{\text{max}}$  in Fig. 3(e). This relationship between  $E_{\text{ph}}^0$  and  $F_{\text{max}}$  is used as a transfer function to convert the measured peak positions [Fig. 2(b)] into estimated  $F_{\text{max}}$  values, which are plotted as a function of the experimentally applied bias ( $V_{\text{expt.}}$ ) in Fig. 3(f). We see clear evidence of a field limit from this spectral data; the spectrally determined value of  $F_{\text{max}}$  does not increase continuously with  $V_{\text{expt.}}$  and reaches a saturated value precisely at the theoretical breakdown limit of  $\beta$ -Ga<sub>2</sub>O<sub>3</sub>, i.e., about 6 MV/cm [23,24]. Notably, our analysis above makes no assumptions about the breakdown limit, and the field values in Fig. 3(f) are entirely based on the measured photocurrent spectra modeled using the XFK effect and the exciton parameters of  $\beta$ -Ga<sub>2</sub>O<sub>3</sub> previously described. The dark current of the Schottky diode is measured with increasing reverse bias, as shown in Fig. 3(g). As expected, the current starts to decrease faster with increasing  $V_{\text{expt.}}$  just where the saturation behavior of  $F_{\text{max}}$  begins in Fig. 3(f).

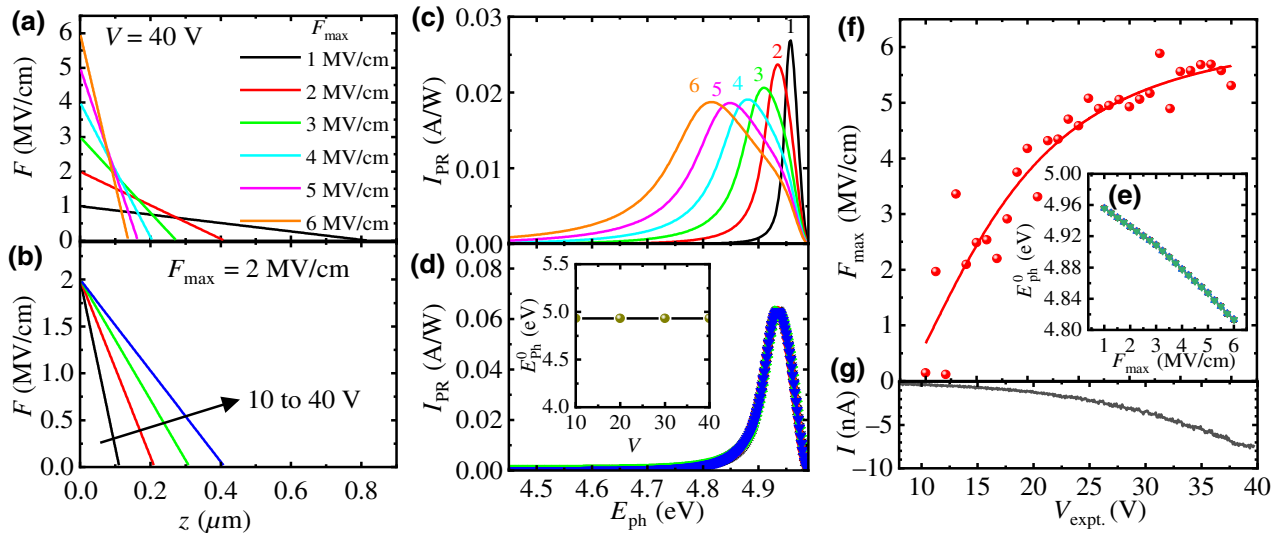


FIG. 3. Spectral observation of the breakdown limit of  $\beta$ -Ga<sub>2</sub>O<sub>3</sub> by local electric field ( $F$ ) measurement. Two hypothetical electrostatic conditions are simulated. (a) Field profiles  $F(z)$  with varying peak field values ( $F_{\text{max}}$ ), but with applied bias ( $V$ ) held constant. (b)  $F(z)$  with constant  $F_{\text{max}}$ , but varying  $V$ . (c), (d) Photoresponsivity spectra modeled using Eqs. (2)–(4) (assuming  $\eta = 1$ ) are plotted for the field profiles shown in (a), (b), respectively. (e) Peak position ( $E_{\text{ph}}^0$ ) extracted from simulated spectra of (c) and plotted as a function of  $F_{\text{max}}$ , demonstrating  $E_{\text{ph}}^0$  as a spectral detector of  $F_{\text{max}}$ . (f) Data from Fig. 2(b) are replotted by using (e) as a transfer function to convert the spectrally measured  $E_{\text{ph}}^0$  values into estimated  $F_{\text{max}}$  values that are then plotted as a function of the experimentally applied reverse bias ( $V_{\text{expt.}}$ ). Spectrally estimated  $F_{\text{max}}$  saturates near the theoretical breakdown field of  $\beta$ -Ga<sub>2</sub>O<sub>3</sub> before global device breakdown is observed. Line is a guide to the eye. (g) Dark  $I$ - $V$  of the device shows the beginning of breakdown, which occurs between 40 and 60 V.

The expected reverse breakdown will happen at around  $40V < V_{\text{expt.}} < 60V$  [72].

Because the photocurrent is excited at the focal point of optical excitation at a particular  $(x, y)$  position on the SBD surface, the observed saturation of  $F_{\text{max}}$  at  $V_{\text{exp}} > 30V$  is a locally measured phenomenon. In this field range, where local-field saturation is observed, near or at the onset of dielectric breakdown, the global device still does not exhibit any current spiking, which occurs in devices processed from this same wafer at  $40V < V_{\text{expt.}} < 60V$ . At the  $(x, y)$  position of the  $I_{\text{PR}}$  measurements, the local  $F_{\text{max}}$  increases evermore slowly with applied bias in the range  $30V < V_{\text{expt.}} < 40V$ , and therefore,  $F_{\text{max}}$  must necessarily be increasing in other regions of the device that have not yet reached the breakdown limit. Thus, this measurement is sensitive to local-field nonuniformity and could be used to map out likely breakdown pathways without destroying devices.

### III. NONLINEAR FIELD-DEPENDENT PHOTOCURRENT AMPLITUDE

The amplitude variation observed in Fig. 2(g) is explained by a field-dependent  $\eta$ , discussed below, due to exciton dissociation and self-trapped hole ionization.

#### A. Field-dependent photocurrent-production pathways: Rate equations

The proposed photocurrent-generation mechanism is illustrated in Fig. 4, with two possible pathways. Both begin by below-band-gap photons absorbed in  $\beta\text{-Ga}_2\text{O}_3$  producing free  $X$ , consisting of a conduction-band electron and a valence-band hole that are mutually bound by  $E_X^0 = 180 - 270$  meV [60,61]. Due to the polaron-formation affinity [63] and large effective mass [42,60,61] of holes, the photoexcited holes cause a lattice distortion that induces a short-range trapping potential for the holes, forming a STH within  $\tau_{\text{ST}} < 0.5$  ps at 295 K [67]. Thus,  $X$  that are not dissociated (path 1) become STXs (path 2) consisting of a conduction-band electron bound to a STH. The  $X$  can also recombine, but this timescale ( $> 1 \mu\text{s}$ ) [66] is much greater than  $\tau_{\text{ST}}$  due to the indirect band gap, and therefore, there is negligible  $X$  recombination, a conclusion also supported by the lack of any reports of free- $X$  photoluminescence, i.e., lack of emission peak at about 4.6 eV in  $\beta\text{-Ga}_2\text{O}_3$ . The fraction of  $X$  that dissociate into free carriers along path 1 is, therefore,  $\eta_X = D_X / (D_X + \tau_{\text{ST}}^{-1})$ , where  $D_X$  is the field-dependent dissociation rate of  $X$ .

At steady state, charge neutrality requires that photoelectron and photohole currents be identical. Given the larger effective mass of holes than of electrons, we assume that the photocurrent is limited by photohole collection. Free holes have an average mobility of  $20 \text{ cm}^2/(\text{Vs})$ ,

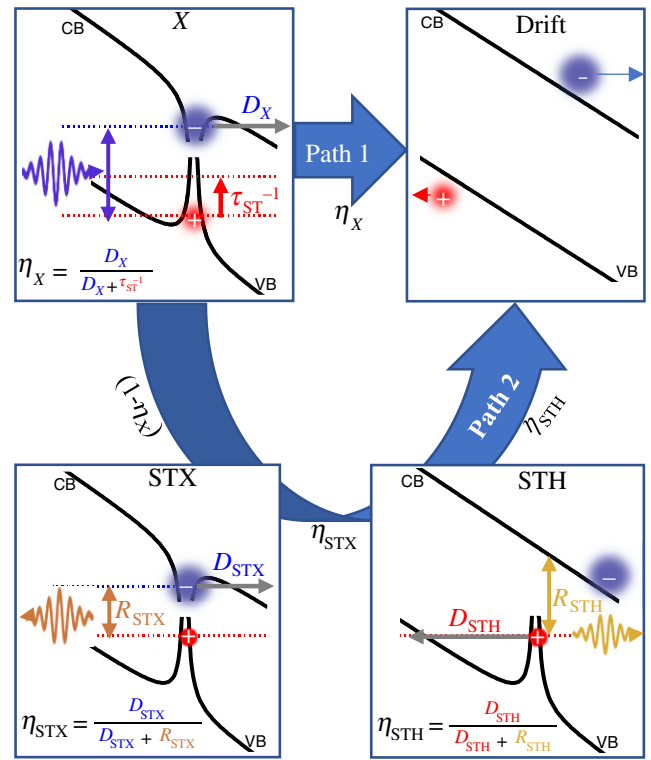


FIG. 4. Photocurrent-production pathways in  $\beta\text{-Ga}_2\text{O}_3$  due to field-induced neutral free- $X$  dissociation and carrier-ionization processes.  $X$  dissociate at rate  $D_X$  by  $e$  tunneling into the CB, generating free electrons and holes that drift to the electrodes along photocurrent path 1. Alternatively, holes can become self-trapped at rate  $\tau_{\text{ST}}^{-1}$ , forming STX, which themselves are dissociated by  $e$  tunneling at rate  $D_{\text{STX}}$ ; otherwise, they recombine at rate  $R_{\text{STX}}$ . If STX dissociate, they leave behind a STH that itself can either dissociate at rate  $D_{\text{STH}}$  by  $h$  tunneling into the VB; otherwise, they recombine with free electrons at rate  $R_{\text{STH}}$ . Path 1 is preferred at low field with a probability of  $\eta_1 = \eta_X$ , while path 2 becomes possible at high field with a probability of  $\eta_2 = (1 - \eta_X)\eta_{\text{STX}}\eta_{\text{STH}}$ .

as recently reported [79], which is consistent with earlier measurements of long minority hole-diffusion lengths of about 200–300 nm [74]. With depletion widths of  $< 1000$  nm, the electron and hole drift times are  $< 1$  ps (assuming saturation velocities  $\geq 10^6$  cm/s), while the free carrier-recombination times are about 210 ps [74]. Thus, the collection efficiency of free electrons or holes is about 100% over the experimental field range, and the total quantum efficiency of path 1 is  $\eta_1 = \eta_X = D_X / (D_X + \tau_{\text{ST}}^{-1})$ .

The fraction of  $X$  that become STXs along path 2 is  $(1 - \eta_X)$ . Within the STXs, the large lattice distortion binds the hole by 490 meV [64], localizing it within a single bond length centered over an oxygen anion, rendering it immobile [16,42,44,63]. As the total STX binding energy is 680 meV [64], within the STX quasi-particle, the electron is bound to the STH by  $(680-490) = 190$  meV. As this energy is much smaller than the STH binding



energy, STX dissociation occurs by the electron tunneling into the conduction band at a field-dependent rate of  $D_{\text{STX}}$ . The fraction of STXs that are dissociated is  $\eta_{\text{STX}} = D_{\text{STX}}/(D_{\text{STX}} + R_{\text{STX}})$ , where  $R_{\text{STX}}$  is the STX recombination rate ( $\sim 10^6 \text{ s}^{-1}$ ) [66]. To produce any current at steady state, the remaining STH must be field ionized (490 meV) at a rate of  $D_{\text{STH}}$  to generate mobile free holes at an efficiency of  $\eta_{\text{STH}} = D_{\text{STH}}/(D_{\text{STH}} + R_{\text{STH}})$ . The total fraction of  $X$  that become STXs and subsequently contribute to current (path 2) is thus  $\eta_2 = (1 - \eta_X)\eta_{\text{STX}}\eta_{\text{STH}}$ .

To validate this model, a relationship between  $F$  and  $\eta$  is derived and compared with the measured  $I_{\text{PR}}^0$ . From the spectral  $E_{\text{ph}}^0$  data combined with the Stark-modified XFK model, a relationship between  $V_{\text{expt.}}$  and  $F_{\text{max}}$  is established, Fig. 3(f). Utilizing this relationship, the  $I_{\text{PR}}^0$  data in Fig. 2(c) are replotted as a function of  $F_{\text{max}}$  in Fig. 5(a). A sudden thresholdlike increase of amplitude at about 4.5 MV/cm is observed. The total IQE is  $\eta = \eta_1 + \eta_2$ . However, if we assume that  $\tau_{\text{ST}} \sim 0.5 \text{ ps}$  [67], then  $\eta_1 \gg \eta_2$  over the entire field range and negligible current would be produced along path 2 at all field values. Data in Fig. 5(a) indicate this is not the case. We hypothesize that  $X$  dissociation (path 1) dominates photocurrent generation in  $\beta$ -Ga<sub>2</sub>O<sub>3</sub> at lower fields, and STX dissociation plus STH field ionization (path 2) must dominate at higher fields, i.e.,  $\eta_2$  turns on at about 4.5 MV/cm.

## B. Field-dependent tunnel ionization rates of excitons and self-trapped holes

The field-induced tunnel ionization rates for excitons ( $D_X$ ), self-trapped excitons ( $D_{\text{STX}}$ ), and self-trapped holes ( $D_{\text{STH}}$ ) are quantitatively modeled utilizing the field-ionization model of impurities proposed by Chaudhuri *et al.* [80,81]. We note the astonishing similarities of  $\beta$ -Ga<sub>2</sub>O<sub>3</sub> excitons (a light electron bound to a very heavy self-trapped hole) with hydrogenic impurities treated by Chaudhuri *et al.*'s model. Indeed, the exciton dissociation problem was treated previously with models [46,82,83] that matched the hydrogenic exciton picture [84]. The field-dependent tunnel ionization rate is given by

$$D(F) = \omega \left( \frac{\alpha}{F} \right)^{2n^*-1} e^{-\alpha/F}, \quad (5)$$

where  $n^*$  is the effective principle quantum number of the ground state within quantum-defect theory, and

$$\alpha = \frac{4(2m^*)^{1/2} E_B^{3/2}}{3q\hbar},$$

$$\omega = \frac{6^{2n^*} E_B |s(n^*)|^2}{3\hbar\Gamma^2(n^* + 1)},$$

$$|s(n^*)| = \frac{\pi}{\sin(n^*\pi)} \left[ \frac{1}{2} \sum_{m=0}^{\infty} \frac{1}{(n^* - m - 1)^2 (n^* - m)^2} \right]^{-1/2}.$$

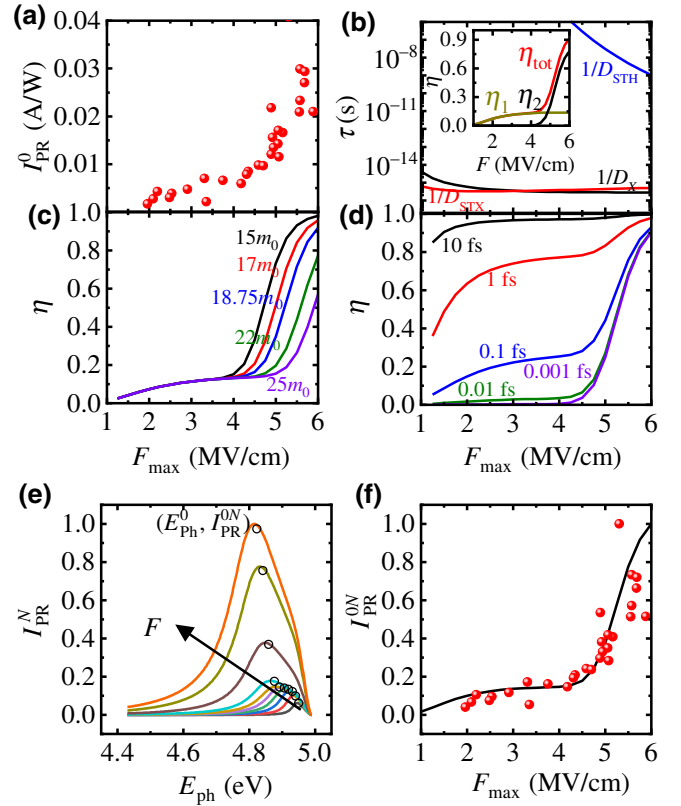


FIG. 5. Field-dependent dissociation of self-trapped excitons and holes in  $\beta$ -Ga<sub>2</sub>O<sub>3</sub>. (a) Photoresponsivity peak amplitude ( $I_{\text{PR}}^0$ ) as a function of field maximum ( $F_{\text{max}}$ ) obtained by replotting data from Fig. 2(c) and converting the experimental reverse bias to  $F_{\text{max}}$  using Fig. 3(f). (b) Dissociation times as a function of  $F$  calculated using Eq. (5). Inset, resulting quantum efficiencies of the two photocurrent production paths (see Fig. 4) as a function of  $F$ . Total quantum efficiency,  $\eta$ , as a function of field  $F$  with varying (c) hole effective mass ( $m_h^*$ ) and (d) self-trapping time ( $\tau_{\text{ST}}$ ), illustrating the sensitivity of the exciton and self-trapped hole field-ionization model to these material parameters. (e) Normalized photoresponsivity ( $I_{\text{PR}}^N$ ) spectra at various  $F$  modeled using Eqs. (2)–(5), i.e.,  $\eta(F) \neq 1$ . (f) Normalized  $I_{\text{PR}}^N$  as a function of  $F$ , comparing data and the best fit. Data are from (a) and theory from (e), where  $I_{\text{PR}}^0$  is normalized by the maximum value of  $I_{\text{PR}}^0$ .

The reduced effective mass ( $\mu_{\text{ex}}$ ,  $m_e^*$ , or  $m_h^*$ ) is  $m^*$  and  $F$  is set equal to  $F_{\text{max}}$ . One should note that, unlike the Merkulov model, the Chaudhuri model incorporates the Stark effect [85]. Thus, incorporating the  $bF^2$  term into  $E_B$  would be redundant, i.e.,  $E_B = E_x^0$ . The noninteger effective principle quantum number ( $n^*$ ) corrects for deviations from the purely hydrogenic case ( $n^* = 1$ ), and is estimated by [81]

$$E_B[\text{eV}] = \frac{m^* 13.6}{m_0 (Kn^*)^2}. \quad (6)$$

For  $X$ , with  $E_B = E_x^0 = 270 \text{ meV}$  [60],  $\mu_{\text{ex}} = 0.3 m_0$  [60], and  $K = K^* = 3.99$  [60], then  $n^* = 0.97$ . In the case of

STXs, replacing  $E_B = E_x^0 = 680 - 490 = 190$  meV [65,66], then  $n^* = 1.16$ . Both values of  $n^*$  are fairly minor deviations from ideal hydrogenic states, which is consistent with  $X$  and STX Bohr radii ( $a_B = 0.70$  nm) that are several bond lengths (0.19 nm) [86]. However, when the light electron is no longer present, as in the case of STHs, all that remains is the highly localized heavy hole, which is expected to exhibit deep-level behavior along with a local lattice distortion (polarization). In this case, an effective dielectric constant ( $K_{\text{STH}}$ ) is not known and neither is the effective mass of the host  $\beta$ -Ga<sub>2</sub>O<sub>3</sub> valence band ( $m_h^*$ ). From previous reports in literature, no conclusion can be drawn about its value, except that it is  $>10 m_0$  [60,61].

There are several recent *ab initio* atomistic models of the STH in  $\beta$ -Ga<sub>2</sub>O<sub>3</sub> that provide a definite length scale for lattice distortion associated with the STH by calculating the probability density function of the hole, which occupies a  $p$  orbital of an O<sup>2-</sup> site [87–89]. From these calculations,  $a_B$  of the STH is roughly half the average interionic bond length, indicating a strong departure from the hydrogenic cases of  $X$  and STXs. Guided by these first-principles calculations, we consider  $a_B^* = 0.06 - 0.14$  nm, which limits the range of  $K_{\text{STH}} m_0 / m_h^* = 1.1 - 2.7$ . Under this constraint, Eqs. (5)–(6) can be used to calculate  $D_{\text{STH}}$  with only one unknown parameter,  $m_h^*$ . As will be discussed below, good-quality fits ( $R^2 \geq 0.9$ ) are obtained for a range of  $m_h^* = 18 - 25 m_0$  for the considered range of  $a_B^*$ . However, the highest-quality fit ( $R^2 \sim 0.92$ ) is obtained for  $m_h^* = 18.8 m_0$ , with  $a_B^* = 0.127$  nm ( $K_{\text{STH}} = 45$  and  $n^* = 0.51$ ). The reduced  $n^*$  and increased effective  $K$  are consistent with a deep level in a distorted dielectric environment.

Utilizing Eq. (5) with  $m_h^* = 18.8 m_0$  ( $n^* = 0.51$ ) and  $\tau_{\text{ST}} = 0.045$  fs,  $D_X$ ,  $D_{\text{STX}}$ , and  $D_{\text{STH}}$  as a function of  $F$  are calculated. The inverses of these rates, i.e., dissociation times, are plotted on a logarithmic scale in Fig. 5(b). Clearly,  $D_{\text{STH}}$  (tunnel ionization of self-trapped holes) is the rate-limiting process for photocurrent generation. We obtain quantum efficiencies for both paths ( $\eta_1$  and  $\eta_2$ ), which are plotted in the inset of Fig. 5(b). The rise in experimentally measured  $I_{\text{PR}}^0$  at about 4.5 MV/cm is obtained from the behavior of path 2 (STX  $\rightarrow$  STH  $\rightarrow$  free carriers). Path 1 ( $X$  dissociation) dominates the photocurrent at low field, where the STHs produced along path 2 cannot be ionized quickly enough to avoid recombination, but, at sufficiently large fields, path 2 can contribute once  $D_{\text{STH}}$  outpaces  $R_{\text{STH}}$ .

The hole effective mass,  $m_h^*$ , strongly impacts the tunneling rate of holes out of the self-trapping potential [Eq. (5)], and therefore,  $m_h^*$  is well determined by the threshold field at which path 2 begins to contribute to photocurrent. This is illustrated in Fig. 5(c); keeping  $\tau_{\text{ST}} = 0.045$  fs, if  $m_h^* < 17.5 m_0$ , path 2 turn on happens too early ( $<4$  MV/cm), while for  $m_h^* > 25.5 m_0$  turn on happens too late ( $>5$  MV/cm). The best-fit hole mass ( $m_h^* =$

$18.8 m_0$ ) matches the observed  $I_{\text{PR}}^0$  high-field turn on at about 4.5 MV/cm.

The self-trapping time ( $\tau_{\text{ST}}$ ) of holes determines if any photocarriers can follow path 2 (i.e.,  $\eta_1/\eta_2$ ), and thus, the ratio of the low-field (path 1) and high-field (path 2) photocurrent magnitudes. This is illustrated in Fig. 5(d); keeping  $m_h^* = 18.8 m_0$ , if  $\tau_{\text{ST}}$  is  $<0.01$  fs, the low-field photocurrent is too small, while, if  $\tau_{\text{ST}}$  is  $>1$  fs, then no high-field turn on is observed. We note that the estimated  $\tau_{\text{ST}} = 0.045$  fs is consistent with the ultrafast pump-probe absorption data in Ref. [67], which is taken at lower photon energies, noting the time-resolution limitation of those experiments. Using this field-dependent model of  $\eta$ , Fig. 5(e) shows the modeled  $I_{\text{PR}}$  spectral behavior at varying  $F$  values. The calculated  $I_{\text{PR}}^0$  values are normalized by the highest-field value and plotted as a function of  $F$  in Fig. 5(f). The model (line) shows a good match to the normalized data (points) taken from Fig. 5(a).

#### IV. CONCLUSIONS AND OUTLOOK

The optoelectronic properties of ultrawide-band-gap low-symmetry materials, like  $\beta$ -Ga<sub>2</sub>O<sub>3</sub>, are far less explored compared with other well-established semiconductors. Using a rather simple measurement (photocurrent spectroscopy in the sub-band-gap regime), a deeper understanding of electron-hole interactions in the strong-field limit is obtained. Just as in 2D TMDs [14,50], the electron-hole interaction in  $\beta$ -Ga<sub>2</sub>O<sub>3</sub> takes on a 2D hydrogen-like geometry, leading to strong polarizabilities combined with large exciton-binding energies. The result is that, under large electric fields, the electron-hole interaction becomes even stronger, i.e., the Stark effect, leading to a prominent redshift of the exciton-absorption peak.

The exciton peak position is shown in  $\beta$ -Ga<sub>2</sub>O<sub>3</sub> to serve as an accurate sensor of the electric field maximum in a Schottky diode structure. We observe a local electric field saturation effect, where the local field does not increase past about 6 MV/cm (nearly the breakdown field of  $\beta$ -Ga<sub>2</sub>O<sub>3</sub>), even though the experimentally applied bias increases (as does the photocurrent amplitude), indicating that this technique can be used to map out field nonuniformity and explore the onset of dielectric breakdown in a nondestructive manner, before actual device breakdown (current spiking) occurs.

Not only does this measurement provide a simple spectral means to track the local field, but the amplitude of the photocurrent versus electric field reveals a very unusual field-dependent quantum efficiency. At about 4.5 MV/cm, the peak amplitude shows an abrupt turn on (threshold). This nonlinear phenomenon is understood by developing the photocurrent rate equations for  $\beta$ -Ga<sub>2</sub>O<sub>3</sub> considering the free- $X$ , STX, and STH field-dependent dissociation rates and ionization rates. As the excitons and STH in  $\beta$ -Ga<sub>2</sub>O<sub>3</sub> are strongly bound, and the effective masses

of holes are large, a deep-tunneling-based field-ionization model is employed to model the ionization rates. Using literature values of the carrier lifetimes, the amplitude variation with field is fitted to estimate two fundamental properties of the  $\beta$ -Ga<sub>2</sub>O<sub>3</sub> valence band: the hole effective mass ( $18.8 m_0$ ) and the hole self-trapping time (0.045 fs), assuming a STH Bohr radius of 0.127 nm. Although this simplistic isotropic model ignores the anisotropy of the STH state, the results are consistent with previous atomistic *ab initio* studies, which are indicative of STHs localized within 0.06 – 0.14 nm. Within quantum-defect theory, we find a reduced effective principle quantum number,  $n^* = 0.51$ , which is consistent with the STH exhibiting deep-level character and an increased polarizability due to local ionic distortion.

For a long time, strong-field exciton physics in three-dimensional (3D) solids has evaded direct measurement and quantitative modeling. This is partly due to the scarcity of 3D materials with simultaneously large  $E_x$  and  $a_B$  and partly due to limitations arising from smaller breakdown fields, even when such materials can be found. As a result, this regime of exciton field-polarization physics is reported only for 1D quantum wires and more recently in 2D TMD materials [14,50,90]. Even then, the models can only qualitatively explain the results, unless complex numerical methods are employed. However, in  $\beta$ -Ga<sub>2</sub>O<sub>3</sub>, the exciton Stark and Franz-Keldysh phenomena can be explained using a simple modified Wannier-Mott-based model [36,39,81]. With the advent of a nondestructive optoelectronic method to measure electric fields based on a spectral peak position, it may become more routine to quantify and study excitonic-absorption- and -dissociation-mediated photocurrent-generation processes in semiconductors with strongly bound and anisotropic excitons.

## ACKNOWLEDGMENTS

Funding for this research is provided by the Center for Emergent Materials, an NSF MRSEC under Grant No. DMR-1420451, and by the AFOSR GAME MURI (Grant No. FA9550-18-1-0479, Program Manager Dr. Ali Sayir).

- 
- [1] E. M. L. D. De Jong, H. Rutjes, J. Valenta, M. T. Trinh, A. N. Poddubny, I. N. Yassievich, A. Capretti, and T. Gregorkiewicz, Thermally stimulated exciton emission in Si nanocrystals, *Light Sci. Appl.* **7**, 17133 (2018).
- [2] G. G. Macfarlane, T. P. McLean, J. E. Quarrington, and V. Roberts, Exciton and phonon effects in the absorption spectra of germanium and silicon, *J. Phys. Chem. Solids* **8**, 388 (1959).
- [3] G. H. Wannier, The structure of electronic excitation levels in insulating crystals, *Phys. Rev.* **52**, 191 (1937).
- [4] N. F. Mott, On the absorption of light by crystals, *Proc. R. Soc. A* **167**, 384 (1938).
- [5] K. L. Shaklee and R. E. Nahory, Valley-Orbit Splitting of Free Excitons? The Absorption Edge of Si, *Phys. Rev. Lett.* **24**, 942 (1970).
- [6] T. P. McLean and R. Loudon, Exciton energy levels in germanium and silicon, *J. Phys. Chem. Solids* **13**, 1 (1960).
- [7] J. Frenkel, On pre-breakdown phenomena in insulators and electronic semi-conductors [3], *Phys. Rev.* **54**, 647 (1938).
- [8] N. Itoh and K. Tanimura, Radiation effects in ionic solids, *Radiat. Eff.* **98**, 269 (1986).
- [9] R. T. Williams and M. N. Kabler, Excited-state absorption spectroscopy of self-trapped excitons in alkali halides, *Phys. Rev. B* **9**, 1897 (1974).
- [10] D. Frohlich and B. Stagninus, New Assignment of the Band Gap in the Alkali Bromides by Two Photon Spectroscopy, *Phys. Rev. Lett.* **19**, 496 (1967).
- [11] M. Inoue, C. K. Mahutte, and S. Wang, Electronic polarons in alkali halides, *Phys. Rev. B* **2**, 539 (1970).
- [12] J. T. Devreese, A. B. Kunz, and T. C. Collins, A resonance of the electronic polaron appearing in the optical absorption of alkali halides, *Solid State Commun.* **11**, 673 (1972).
- [13] B. Scharf, T. Frank, M. Gmitra, J. Fabian, I. Žutić, and V. Perebeinos, Excitonic stark effect in MoS<sub>2</sub> monolayers, *Phys. Rev. B* **94**, 245434 (2016).
- [14] M. Massicotte, F. Vialla, P. Schmidt, M. B. Lundeberg, S. Latini, S. Hastrup, M. Danovich, D. Davydovskaya, K. Watanabe, T. Taniguchi, V. I. Fal'ko, K. S. Thygesen, T. G. Pedersen, and F. H. L. Koppens, Dissociation of two-dimensional excitons in monolayer WSe<sub>2</sub>, *Nat. Commun.* **9**, 1633 (2018).
- [15] S. Hastrup, S. Latini, K. Bolotin, and K. S. Thygesen, Stark shift and electric-field-induced dissociation of excitons in monolayer MoS<sub>2</sub> and h BN/MoS<sub>2</sub> heterostructures, *Phys. Rev. B* **94**, 041401 (2016).
- [16] G. Wang, A. Chernikov, M. M. Glazov, T. F. Heinz, X. Marie, T. Amand, and B. Urbaszek, Colloquium: Excitons in atomically thin transition metal dichalcogenides, *Rev. Mod. Phys.* **90**, 021001 (2018).
- [17] Y. Lin, X. Ling, L. Yu, S. Huang, A. L. Hsu, Y. H. Lee, J. Kong, M. S. Dresselhaus, and T. Palacios, Dielectric screening of excitons and trions in single-layer MoS<sub>2</sub>, *Nano Lett.* **14**, 5569 (2014).
- [18] J. Pei, J. Yang, R. Xu, Y. H. Zeng, Y. W. Myint, S. Zhang, J. C. Zheng, Q. Qin, X. Wang, W. Jiang, and Y. Lu, Exciton and trion dynamics in bilayer MoS<sub>2</sub>, *Small* **11**, 6384 (2015).
- [19] C. Yang, Y. Gao, C. Qin, X. Liang, S. Han, G. Zhang, R. Chen, J. Hu, L. Xiao, and S. Jia, All-optical reversible manipulation of exciton and trion emissions in monolayer WS<sub>2</sub>, *Nanomaterials* **10**, 23 (2020).
- [20] J. Yang, R. Xu, J. Pei, Y. W. Myint, F. Wang, Z. Wang, S. Zhang, Z. Yu, and Y. Lu, Optical tuning of exciton and trion emissions in monolayer phosphorene, *Light Sci. Appl.* **4**, e312 (2015).
- [21] C. H. Lui, A. J. Frenzel, D. V. Pilon, Y. H. Lee, X. Ling, G. M. Akselrod, J. Kong, and N. Gedik, Trion-Induced Negative Photoconductivity in Monolayer MoS<sub>2</sub>, *Phys. Rev. Lett.* **113**, 166801 (2014).
- [22] H. Masataka, S. Kohei, M. Hisashi, K. Yoshinao, K. Akinori, K. Akito, M. Takekazu, and Y. Shigenobu, Recent progress in Ga<sub>2</sub>O<sub>3</sub> power devices, *Semicond. Sci. Technol.* **31**, 034001 (2016).



- [23] X. Yan, I. S. Esqueda, J. Ma, J. Tice, and H. Wang, High breakdown electric field in  $\beta$ -Ga<sub>2</sub>O<sub>3</sub>/graphene vertical barristor heterostructure, *Appl. Phys. Lett.* **112**, 032101 (2018).
- [24] K. D. Chabak, N. Moser, A. J. Green, D. E. Walker, S. E. Tetlak, E. Heller, A. Crespo, R. Fitch, J. P. McCandless, K. Leedy, M. Baldini, G. Wagner, Z. Galazka, X. Li, and G. Jessen, Enhancement-mode Ga<sub>2</sub>O<sub>3</sub> wrap-gate Fin field-effect transistors on native (100)  $\beta$ -Ga<sub>2</sub>O<sub>3</sub> substrate with high breakdown voltage, *Appl. Phys. Lett.* **109**, 213501 (2016).
- [25] W. Y. Kong, G. A. Wu, K. Y. Wang, T. F. Zhang, Y. F. Zou, D. D. Wang, and L. B. Luo, Graphene- $\beta$ -Ga<sub>2</sub>O<sub>3</sub> Heterojunction for highly sensitive deep UV photodetector application, *Adv. Mater.* **28**, 10725 (2016).
- [26] D. Guo, Q. Guo, Z. Chen, Z. Wu, P. Li, and W. Tang, Review of Ga<sub>2</sub>O<sub>3</sub>-based optoelectronic devices, *Mater. Today Phys.* **11**, 100157 (2019).
- [27] A. Singh Pratiyush, S. Krishnamoorthy, S. Vishnu Solanke, Z. Xia, R. Muralidharan, S. Rajan, and D. N. Nath, High responsivity in molecular beam epitaxy grown  $\beta$ -Ga<sub>2</sub>O<sub>3</sub> metal semiconductor metal solar blind deep-UV photodetector, *Appl. Phys. Lett.* **110**, 221107 (2017).
- [28] A. S. Pratiyush, S. Krishnamoorthy, S. Kumar, Z. Xia, R. Muralidharan, S. Rajan, and D. N. Nath, Demonstration of zero bias responsivity in MBE grown  $\beta$ -Ga<sub>2</sub>O<sub>3</sub> lateral deep-UV photodetector, *Jpn. J. Appl. Phys.* **57**, 060313 (2018).
- [29] F. Walter, Einfluß eines elektrischen felde Auf eine optische absorptionskante, *Zeitschrift Fur Naturforsch. - Sect. A J. Phys. Sci.* **13**, 484 (1958).
- [30] L. V. Keldysh, The effect of a strong electric field on the optical properties of insulating crystal, *J. Exptl. Theor. Phys.* **34**, 1138 (1958).
- [31] D. E. Aspnes, Electric-Field effects on optical absorption near thresholds in solids, *Phys. Rev.* **147**, 554 (1966).
- [32] T. Maeda, T. Narita, M. Kanechika, T. Uesugi, T. Kachi, T. Kimoto, M. Horita, and J. Suda, Franz-Keldysh effect in GaN p-n junction diode under high reverse bias voltage, *Appl. Phys. Lett.* **112**, 252104 (2018).
- [33] T. Maeda, X. Chi, H. Tanaka, M. Horita, J. Suda, and T. Kimoto, Franz-keldysh effect in 4H-SiC p-n junction diodes under high electric field along the  $\langle 11\bar{2}0 \rangle$  direction, *Jpn. J. Appl. Phys.* **58**, 091007 (2019).
- [34] T. Maeda, T. Narita, H. Ueda, M. Kanechika, T. Uesugi, T. Kachi, T. Kimoto, M. Horita, and J. Suda, Measurement of avalanche multiplication utilizing franz-keldysh effect in GaN p-n junction diodes with double-side-depleted shallow bevel termination, *Appl. Phys. Lett.* **115**, 142101 (2019).
- [35] T. Maeda, X. Chi, M. Horita, J. Suda, and T. Kimoto, Phonon-assisted optical absorption due to franz-keldysh effect in 4H-SiC p-n junction diode under high reverse bias voltage, *Appl. Phys. Express* **11**, 091302 (2018).
- [36] D. Verma, M. M. R. Adnan, M. W. Rahman, S. Rajan, and R. C. Myers, Local electric field measurement in GaN diodes by exciton franz-keldysh photocurrent spectroscopy, *Appl. Phys. Lett.* **116**, 202102 (2020).
- [37] J. D. Dow and D. Redfield, Electroabsorption in semiconductors: The excitonic absorption edge, *Phys. Rev. B* **1**, 3358 (1970).
- [38] D. F. Blossey, Wannier exciton in an electrical field. I. Optical absorption by bound and continuum states, *Phys. Rev. B* **2**, 3976 (1970).
- [39] I. Merkulov, Influence of exciton effect on electroabsorption in semiconductors, *Sov. J. Exp. Theor. Phys.* **39**, 2314 (1974).
- [40] J. Y. Duboz, F. Binet, E. Rosencher, F. Scholz, and V. Härle, Electric field effects on excitons in gallium nitride, *Mater. Sci. Eng. B* **43**, 269 (1997).
- [41] F. Binet, J. Y. Duboz, E. Rosencher, F. Scholz, and V. Härle, Electric field effects on excitons in gallium nitride, *Phys. Rev. B* **54**, 8116 (1996).
- [42] J. B. Varley and A. Schleife, Bethe-salpeter calculation of optical-absorption spectra of In<sub>2</sub>O<sub>3</sub> and Ga<sub>2</sub>O<sub>3</sub>, *Semicond. Sci. Technol.* **30**, 024010 (2015).
- [43] T. Onuma, K. Tanaka, K. Sasaki, T. Yamaguchi, T. Honda, A. Kuramata, S. Yamakoshi, and M. Higashiwaki, Electroreflectance study on optical anisotropy in  $\beta$ -Ga<sub>2</sub>O<sub>3</sub>, *Appl. Phys. Lett.* **115**, 231102 (2019).
- [44] J. Furthmüller and F. Bechstedt, Quasiparticle bands and spectra of Ga<sub>2</sub>O<sub>3</sub> polymorphs, *Phys. Rev. B* **93**, 115204 (2016).
- [45] M. D. Tabak and P. J. Warter, Field-controlled photogeneration and free-carrier transport in amorphous selenium films, *Phys. Rev.* **173**, 899 (1968).
- [46] N. F. Mott and A. M. Stoneham, The lifetime of electrons, holes and excitons before self-trapping, *J. Phys. C Solid State Phys.* **10**, 3391 (1977).
- [47] S. D. Ganichev, I. N. Yassievich, and W. Prettl, Tunnel ionization of deep impurities by Far-infrared radiation, *Semicond. Sci. Technol.* **11**, 679 (1996).
- [48] S. D. Ganichev, E. Ziemann, W. Prettl, and I. Yassievich, Distinction between the poole-frenkel and tunneling models of electric-field-stimulated carrier emission from deep levels in semiconductors, *Phys. Rev. B* **61**, 10361 (2000).
- [49] T. C. Smith, D. L. Pan, and D. S. McGill, Impact ionization of excitons in Ge and Si, *Phys. Rev. B* **12**, 4360 (1975).
- [50] H. C. Kamban and T. G. Pedersen, Field-induced dissociation of two-dimensional excitons in transition metal dichalcogenides, *Phys. Rev. B* **100**, 045307 (2019).
- [51] L. S. R. Cavalcante, D. R. daCosta, G. A. Farias, D. R. Reichman, and A. Chaves, Stark shift of excitons and trions in two-dimensional materials, *Phys. Rev. B* **98**, 245309 (2018).
- [52] G. Weiser, Stark effect of one-dimensional wannier excitons in polydiacetylene single crystals, *Phys. Rev. B* **45**, 14076 (1992).
- [53] A. Horvath, G. Weiser, C. Lapersonne-Meyer, M. Schott, and S. Spagnoli, Wannier excitons and franz-keldysh effect of polydiacetylene chains diluted in their single crystal monomer matrix, *Phys. Rev. B* **53**, 13507 (1996).
- [54] S. Latini, T. Olsen, and K. S. Thygesen, Excitons in van Der Waals Heterostructures: The important role of dielectric screening, *Phys. Rev. B* **92**, 245123 (2015).
- [55] L. Keldysh, Coulomb interaction in thin semiconductor and semimetal films, *Sov. J. Exp. Theor. Phys. Lett.* **29**, 658 (1979).
- [56] H. I. Ralph, The electronic absorption edge in layer type crystals, *Solid State Commun.* **3**, 303 (1965).
- [57] M. Shinada and S. Sugano, Interband optical transitions in extremely anisotropic semiconductors I. bound and



- unbound exciton absorption, *J. Phys. Soc. Japan* **21**, 1936 (1966).
- [58] P. Cudazzo, I. V. Tokatly, and A. Rubio, Dielectric screening in two-dimensional insulators: Implications for excitonic and impurity states in graphane, *Phys. Rev. B* **84**, 085406 (2011).
- [59] T. C. Berkelbach, M. S. Hybertsen, and D. R. Reichman, Theory of neutral and charged excitons in monolayer transition metal dichalcogenides, *Phys. Rev. B* **88**, 045318 (2013).
- [60] F. Bechstedt and J. Furthmüller, Influence of screening dynamics on excitons in Ga<sub>2</sub>O<sub>3</sub> polymorphs, *Appl. Phys. Lett.* **114**, 122101 (2019).
- [61] A. Mock, R. Korlacki, C. Briley, V. Darakchieva, B. Mone-mar, Y. Kumagai, K. Goto, M. Higashiwaki, and M. Schubert, Band-to-band transitions, selection rules, effective mass, and excitonic contributions in monoclinic  $\beta$ -Ga<sub>2</sub>O<sub>3</sub>, *Phys. Rev. B* **96**, 245205 (2017).
- [62] C. Sturm, J. Furthmüller, F. Bechstedt, R. Schmidt-Grund, and M. Grundmann, Dielectric tensor of monoclinic Ga<sub>2</sub>O<sub>3</sub> single crystals in the spectral range 0.5-8.5 eV, *APL Mater.* **3**, 106106 (2015).
- [63] J. B. Varley, A. Janotti, C. Franchini, and C. G. Van De Walle, Role of self-trapping in luminescence and p-type conductivity of wide-band-gap oxides, *Phys. Rev. B* **85**, 081109 (2012).
- [64] S. Yamaoka and M. Nakayama, Evidence for formation of self-trapped excitons in a  $\beta$ -Ga<sub>2</sub>O<sub>3</sub> single crystal, *Phys. Status Solidi* **13**, 93 (2016).
- [65] S. Yamaoka, Y. Mikuni, and M. Nakayama, Photoluminescence Polarization Characteristics of Self-Trapped Excitons in an Undoped  $\beta$ -Ga<sub>2</sub>O<sub>3</sub> Single Crystal. *J. Phys.: Conf. Ser.* **1220**, 012030 (2019).
- [66] S. Yamaoka, Y. Furukawa, and M. Nakayama, Initial process of photoluminescence dynamics of self-trapped excitons in a  $\beta$ -Ga<sub>2</sub>O<sub>3</sub> single crystal, *Phys. Rev. B* **95**, 094304 (2017).
- [67] S. Marcinkevičius and J. S. Speck, Ultrafast dynamics of hole self-localization in  $\beta$ -Ga<sub>2</sub>O<sub>3</sub>, *Appl. Phys. Lett.* **116**, 132101 (2020).
- [68] M. Baldini, Z. Galazka, and G. Wagner, Recent progress in the growth of  $\beta$ -Ga<sub>2</sub>O<sub>3</sub> for power electronics applications, *Mater. Sci. Semicond. Process.* **78**, 132 (2018).
- [69] B. Jogai, Free electron distribution in AlGa<sub>N</sub>/Ga<sub>N</sub> heterojunction field-effect transistors, *J. Appl. Phys.* **91**, 3721 (2002).
- [70] M. Grundmann, *BandEng: Poisson-Schrodinger Solver Software*. <https://my.ece.ucsb.edu/mgrundmann/bandeng/>.
- [71] A. M. Armstrong, M. H. Crawford, A. Jayawardena, A. Ahyi, and S. Dhar, Role of self-trapped holes in the photoconductive gain of  $\beta$ -gallium oxide Schottky diodes, *J. Appl. Phys.* **119**, 103102 (2016).
- [72] See the Supplemental Material at <http://link.aps.org/supplemental/10.1103/PhysRevApplied.16.034011> for a derivation of the photocurrent equation from the optical path, light  $I$ - $V$  diode characterization, XFK effect measurements on additional devices, and frequency-polarization-dependent photocurrent spectra of  $\beta$ -Ga<sub>2</sub>O<sub>3</sub>.
- [73] H. Peelaers and C. G. Van De Walle, Sub-band-gap absorption in Ga<sub>2</sub>O<sub>3</sub>, *Appl. Phys. Lett.* **111**, 182104 (2017).
- [74] J. Lee, E. Flitsyan, L. Chernyak, J. Yang, F. Ren, S. J. Pearton, B. Meyler, and Y. J. Salzman, Effect of 1.5MeV electron irradiation on  $\beta$ -Ga<sub>2</sub>O<sub>3</sub> carrier lifetime and diffusion length, *Appl. Phys. Lett.* **112**, 082104 (2018).
- [75] H. Haug and S. W. Koch, *Quantum Theory Of The Optical And Electronic Properties Of Semiconductors*, 5th ed. (World Scientific Publishing Co., Singapore, 2004).
- [76] Q. Wang, J. Chen, P. Huang, M. Li, Y. Lu, K. P. Homewood, G. Chang, H. Chen, and Y. He, Influence of growth temperature on the characteristics of  $\beta$ -Ga<sub>2</sub>O<sub>3</sub> epitaxial films and related solar-blind photodetectors, *Appl. Surf. Sci.* **489**, 101 (2019).
- [77] H. Sheoran, B. R. Tak, N. Manikanthababu, and R. Singh, Temperature-dependent electrical characteristics of Ni/Au vertical Schottky barrier diodes on  $\beta$ -Ga<sub>2</sub>O<sub>3</sub> epilayers, *ECS J. Solid State Sci. Technol.* **9**, 055004 (2020).
- [78] S. A. O. Russell, A. Perez-Tomas, C. F. McConville, C. A. Fisher, D. P. Hamilton, P. A. Mawby, and M. R. Jennings, Heteroepitaxial  $\beta$ -Ga<sub>2</sub>O<sub>3</sub> on 4H-SiC for an FET with reduced self heating, *IEEE J. Electron Devices Soc.* **5**, 256 (2017).
- [79] F. Akyol, Simulation of  $\beta$ -Ga<sub>2</sub>O<sub>3</sub> vertical Schottky diode based photodetectors revealing average hole mobility of 20 cm<sup>2</sup> V<sup>-1</sup> s<sup>-1</sup>, *J. Appl. Phys.* **127**, 074501 (2020).
- [80] S. Chaudhuri, D. D. Coon, and G. E. Derkits, Quantum-mechanical estimates of the speed of field ionization of shallow impurity levels, *Appl. Phys. Lett.* **37**, 111 (1980).
- [81] S. Chaudhuri, D. D. Coon, and R. P. G. Karunasiri, Impurity-to-band tunneling in semiconductors, *J. Appl. Phys.* **54**, 5476 (1983).
- [82] J. Singh, *Excitation Energy Transfer Processes in Condensed Matter Theory and Applications*, 1st ed. (Springer Science, Darwin, Australia, 1994).
- [83] J. Singh, *Optical Properties of Condensed Matter and Applications - Wiley Series in Materials for Electronic - Amp - Optoelectronic Applications*, 2nd ed. (JohnWiley & Sons Ltd, Darwin, Australia, 2006).
- [84] D. Farrelly and W. P. Reinhardt, Uniform semiclassical and accurate quantum calculations of complex energy eigenvalues for the hydrogen atom in a uniform electric field, *J. Phys. B* **16**, 2103 (1983).
- [85] J. R. Banavar, D. D. Coon, and G. E. Derkits, Low-temperature field ionization of localized impurity levels in semiconductors, *Appl. Phys. Lett.* **34**, 94 (1979).
- [86] K. Imscher, Z. Galazka, M. Pietsch, R. Uecker, and R. Fornari, *Electrical properties of  $\beta$ -Ga<sub>2</sub>O<sub>3</sub> single crystal grown by czochrolaski method*, *J. Appl. Phys.* **110**, 063720 (2011).
- [87] Y. K. Frodason, K. M. Johansen, L. Vines, and J. B. Varley, Self-Trapped hole and impurity-related broad luminescence in  $\beta$ -Ga<sub>2</sub>O<sub>3</sub>, *J. Appl. Phys.* **127**, 075701 (2020).
- [88] T. Gake, Y. Kumagai, and F. Oba, First-Principles study of self-trapped holes and acceptor impurities in Ga<sub>2</sub>O<sub>3</sub> polymorphs, *Phys. Rev. Mater.* **3**, 044603 (2019).
- [89] B. E. Kananen, N. C. Giles, L. E. Halliburton, G. K. Fountos, K. B. Chang, and K. T. Stevens, Self-trapped holes in  $\beta$ -Ga<sub>2</sub>O<sub>3</sub> crystals, *J. Appl. Phys.* **122**, 215703 (2017).
- [90] T. G. Pedersen, Analytical models of optical response in one-dimensional semiconductors, *Phys. Lett. A* **379**, 1785 (2015).